Energy levels and hypersensitivity of samarium(III) in the elpasolite $Cs_2NaSmCl_6$

2006 J. Phys.: Condens. Matter 18 8503

(http://iopscience.iop.org/0953-8984/18/37/009)

INSTITUTE OF PHYSICS PUBLISHING JOURNAL OF PHYSICS: CONDENSED MATTER

J. Phys.: Condens. Matter **18** (2006) 8503–8522 doi:10.1088/0953-8984/18/37/009

Energy levels and hypersensitivity of samarium(III) in the elpasolite $Cs_2NaSmCl_6$

Michèle D Faucher[1] **and Peter A Tanner**[2]

[1] 88 Avenue Jean Jaurès, 92140 Clamart, France
[2] Department of Biology and Chemistry, City University of Hong Kong, Tat Chee Avenue, Kowloon, Hong Kong S.A.R., People's Republic of China

Received 1 June 2006, in final form 31 July 2006
Published 1 September 2006
Online at stacks.iop.org/JPhysCM/18/8503

Abstract

Electronic absorption spectra of *neat* $Cs_2NaSmCl_6$ between 300 and 10 K are reported for the spectral region between 900 and 40 000 cm^{-1}. Interpretation of the intricate vibronic structure enables 91 conclusive and 45 tentative Kramers doublet and quartet energy levels of the $4f^5$ ion Sm^{3+} in this system to be assigned. Configuration interaction assisted crystal field calculations employing the diagonalization of the combined $4f^5$ and $4f^46p^1$ matrices fit the energy levels better than the conventional $4f^5$ crystal field calculation. The $4f^5$ calculation is more accurate, however, than for the Pr^{3+} and Nd^{3+} elpasolite systems, showing the greater importance of intra- rather than inter-configuration interaction for the more complex electronic structure of Sm^{3+}. The experimental dataset generally shows agreement with that from two-photon excitation spectroscopy and the differences are highlighted. The intensity of structure at and near the zero phonon line of the hypersensitive infrared $(^6H_{5/2})\Gamma_7 \rightarrow \Gamma_6(^6F_{1/2})$ absorption transition increases relative to the intensity of the vibronic sideband when z is increased in $Cs_2NaSm(Cl_{1-z}Br_z)_6$. This is attributed to the introduction of electric dipole transition intensity into the pure electronic transition by lowering the site-symmetry of $SmCl_6^{3-}$, or by the presence of $SmCl_5Br^{3-}$.

1. Introduction

The energy levels of Sm^{3+} in the cubic elpasolite host Cs_2NaYCl_6 have been investigated by two-photon excitation (TPE) spectroscopy by Denning and co-workers [1], following previous studies by one-photon absorption [2, 3] and emission [4, 5]. The use of TPE spectroscopy in elucidating the energy levels of the lanthanide ions Eu^{3+} and Tb^{3+} in this lattice proved to be remarkably successful [6, 7]. In the case of Sm^{3+}, 42 levels were assigned from the energy 17 738 cm^{-1} up to 29 000 cm^{-1} from the TPE spectra of Cs_2NaYCl_6:Sm^{3+} [1]. However, the TPE study of this system has some inherent limitations. First, the Sm^{3+} ion only has a transparent window between 11 000 and 17 000 cm^{-1}, thereby providing a maximum upper energy level limit of about 34 000 cm^{-1}. Second, the fact that Sm^{3+} is an odd-electron system,

$4f^5$, gives less-restrictive selection rules for polarized TPE than for Eu^{3+} $4f^6$ and Tb^{3+} $4f^8$. Third, level congestion is acute, with about 80 levels between 21 000 and 28 000 cm^{-1}. Furthermore, the emission from the luminescent probe, $^4G_{5/2}$, is weak.

We consider that the study of the electronic energy levels of Sm^{3+} ion is important in order to understand the mechanisms of the energy transfer processes, such as those in which Sm^{3+} quenches Ho^{3+} [8] and Eu^{3+} [9–12] luminescence. Therefore we have made an investigation using one-photon absorption in order to provide assignments for the crystal field (CF) levels of the $^6H_{13/2}$ and $^6F_{11/2}$ multiplet terms, as well to assign and compare our results for *neat* $Cs_2NaSmCl_6$ with the TPE assignments for CF levels in Cs_2NaYCl_6:Sm^{3+} above 20 000 cm^{-1}. Although the levels are congested, we have exploited the detailed and unique one-phonon sideband fingerprint, the calculated magnetic dipole (MD) intensity ratios of zero phonon lines (ZPLs) in the region below 20 000 cm^{-1}, as well as the temperature dependence of the vibronic and electronic structure, in order to make assignments. Naturally, the two-photon results were a very useful guide in the interpretation of such complex spectra.

However, in order not to confuse the energy level dataset by including energy levels from Cs_2NaYCl_6:Sm^{3+} together with those of $Cs_2NaSmCl_6$, we have focused upon the latter. This enables a clearer comparison of the derived parameters to be made with those from other *neat* hexahaloelpasolites. The $Cs_2NaSmCl_6$ system is cubic, O_h^5 ($Fm3m$), at room temperature [13] but it undergoes a crystallographic phase transition at ≈100 K [14] so that the molecular ion point group symmetry is lowered from octahedral to tetragonal. The C_{4h} CF splittings of Kramers quartets are fortunately small (<10 cm^{-1}), and in some cases these observed splittings enable Kramers quartets to be distinguished from doublets. This clear focus upon the neat $Cs_2NaSmCl_6$ system and the determination of 135 energy levels of total degeneracy 414 for its experimental energy level dataset permits a detailed comparison of the data fits from $4f^5$ and $4f^4np$ energy level calculations in order to assess the importance of configuration interaction (CI) for this system. We have previously found that the introduction of the CI of a $4f^N$ configuration with $4f^{N-1}np$ into the crystal field calculations can greatly increase the accuracy of the energy level fit [15–18]. The $4f^5$ Sm^{3+} system now presents a much more extensive and complex test.

Further interest in the $Cs_2NaSmCl_6$ system arose from the reported hypersensitive transition in the near infrared [3, 19]. We clarify herein the effects of hypersensitivity upon a pure electronic electric quadrupole (EQ) transition and upon the associated vibronic structure because the distinction has not always been made between these effects [20–24].

After a brief review of experimental details (section 2), the absorption spectra are presented in section 3. The configuration interaction assisted crystal field (CIACF) calculation is presented in section 4 and the main conclusions are itemized in section 5.

2. Experiment

Polycrystalline samples of the neat elpasolite $Cs_2NaSmCl_6$ and bromide doped samples, $Cs_2NaSm(Br_zCl_{1-z})_6$ (where nominally $z = 0.04, 0.05, 0.075, 0.1, 0.2, 0.25$), were prepared by the method E of Morss *et al* [13], sealed in quartz ampoules under vacuum, and grown by the Bridgman technique. The concentration of bromide ion was determined by a Dionex ion chromatography module. Since during the preparation of these materials the NaBr was added together with NaCl into the concentrated HCl mixture, and this was subsequently taken to dryness, the nominal concentrations of Br in $Cs_2NaSm(Br_zCl_{1-z})_6$ were much greater than the actual concentrations measured by ion chromatography (e.g. for the nominal $Cs_2NaSm(Cl_{0.75}Br_{0.25})_6$ sample the actual formula was near $Cs_2NaSm(Cl_{0.96}Br_{0.04})_6$. In fact a quadratic relationship was found from five samples between the measured (y) and the

nominal concentrations (x = at.%Br = $100z$) in the range up to nominal Cl:Br = 3.0: $y = 0.1129 + 0.0049x + 0.0054x^2$ ($R^2 = 0.9666$).

Infrared absorption spectra from 600 to 6000 cm^{-1} were recorded at 300 K and ca 90 K using a Bomem MB-120 Spectrometer equipped with a Specac variable temperature cell. Absorption spectra using various lamps in the range 3000–30 000 cm^{-1} were recorded between 300 and 10 K using a Biorad FTS-60A Spectrometer, equipped with PbSe, silicon and photomultiplier detectors, with the sample housed in an Oxford Instruments closed-cycle cryostat. Ultraviolet absorption spectra (25 000–45 000 cm^{-1}) were recorded in the single-beam mode by a back-illuminated SpectruMM CCD detector with an Acton 0.5 m monochromator equipped with an 1800 g mm^{-1} grating blazed at 250 nm, using a xenon or deuterium lamp as excitation source.

Finally a technical point is made. Our measurements from Fourier transform spectra (mostly in the range below 20 000 cm^{-1}), where the wavenumber is directly measured, are more accurate than those in the ultraviolet. The difference at the energy 35 000 cm^{-1} between air and vacuum wavenumbers is ~10 cm^{-1}. However, the conversion from air to vacuum wavelengths assumes 'standard air', for which the ambient conditions are seldom met. The comparison of measured energies of ultraviolet spectral features in previous absorption spectral studies of $Cs_2NaSmCl_6$ and in the present work (referred to in section 3.6) show that differences of up to 17–34 cm^{-1} exist, which are larger magnitudes than the mean deviation of the present energy level calculation.

3. Results and discussion

The initial state in the 10 K absorption transitions of Sm^{3+} in $Cs_2NaSmCl_6$ is $(^6H_{5/2})\Gamma_7$. The next-highest $^6H_{5/2}$ level, Γ_8 at 165 cm^{-1}, is appreciably populated at liquid nitrogen temperature. The site selection rules in the O_h^* double group for pure electronic transitions between CF levels permit the introduction of MD character, except for transitions from Γ_7 to excited Γ_6 levels. The identification of excited states via absorption spectroscopy is thereby facilitated by the direct observation of ZPLs in most cases, and in the region below 20 000 cm^{-1} the intensity ratios of transitions to terminal states within a given multiplet term have been compared with those calculated from the tabulated MD line strengths of Morrison and Leavitt [25] and previous studies [2, 4]. These line strengths are approximate for two reasons, but serve to discriminate between alternative symmetry assignments of levels in most cases. First, the eigenvectors of the initial crystal field fitting in [25] are not very accurate and the parentage of levels is mixed, with major eigenvector components <30% of the total in many cases [4]. Second, the deviation from octahedral symmetry of the system is not included.

Confirmation of an excited state energy location, other than by the ZPL assignment, is provided by the location of the vibronic sideband fingerprint to high energy. The energies (in cm^{-1}) of vibronic structure in the electronic spectra of $Cs_2NaSmCl_6$ are: S_5 (Cs^+ translation, τ_{2g}) 40; S_9 (Cs^+ translation, τ_{1u}) 58; $S_7\nu_4$ (Cl–Sm–Cl bend, τ_{1u}) 99, 125; $S_{10}\nu_6$ (Cl–Sm–Cl bend, τ_{2u}) 72, 81; S_8 (Na–Cl stretch, τ_{1u}) 180; and $S_6\nu_3$ (Sm–Cl stretch, τ_{1u}) 238, 252, 280, where the unit cell group vibrations are labelled in the notation of Lentz [26] and the ungerade $SmCl_6^{3-}$ moiety mode vibrations are labelled ν_i. The interpretation of this structure in terms of zone boundary modes and transverse–longitudinal splittings has previously been debated and is not included herein [2–5]. The substructure within each vibronic origin is observed to differ in relative intensity for the absorption transitions to terminal states of different symmetry irreps.

The spectra recorded in this study extend from the infrared to ultraviolet regions and are very extensive. Absorption spectra of selected transitions of $Cs_2NaSmCl_6$ are illustrated in figure 1, and the derived electronic energy levels are listed in table 1. The comparison with the TPE results for $Cs_2NaYCl_6:Sm^{3+}$ [1] which extend up to level 137, assigned at 28 156 cm^{-1},

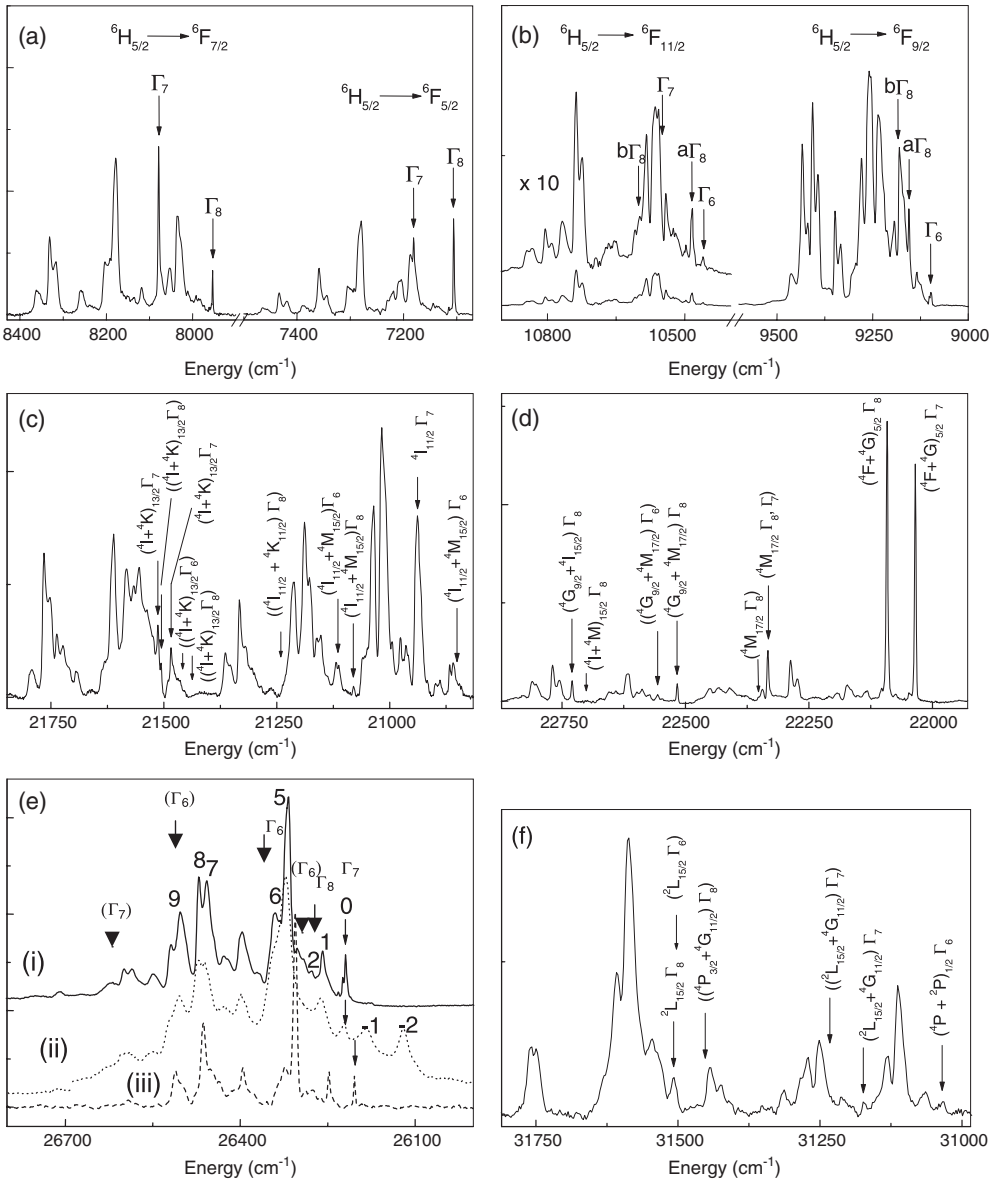

Figure 1. Selected absorption spectra of $Cs_2NaSmCl_6$ at 10 K. The ordinate throughout is absorbance. The initial state is $^6H_{5/2}\Gamma_7$. The electronic origins are marked with the irreps of the terminal electronic states. Note the breaks in the energy scales. In (e), the 10 K (i) and 60 K (ii) spectra of $Cs_2NaSmCl_6$ are shown, together with the 10 K spectrum of $Cs_2NaY_{0.9}Sm_{0.1}Cl_6$ (iii). The numbered bands in (e) (with one exception, −1) relate to the $\Gamma_7 \rightarrow \Gamma_7$ transition and are assigned in table 2.

is also included in table 1. The results of the calculation in [1] are very similar to those of the $4f^5$ calculation in [27] and the ordering of levels is the same, except that the levels 109, 110 are interchanged, as are 120 and 121.

The detailed arguments for the assignments from the one-photon absorption spectra are often intricate [28] so that only a brief overview and description of the results is presented in

Table 1. Observed and calculated energy level scheme for Sm^{3+} in $Cs_2NaSmCl_6$.

Level no.	Multiplet term[a]	CF level[b]	Obs. [1][c] Denning	Obs. this study[d]	Calc.[e]	Δ[f]
1	$^6H_{5/2}$	Γ_7	0	0	−12	12
2	$^6H_{5/2}$	Γ_8	166	165	155	10
3	$^6H_{7/2}$	Γ_6	1 046	1 044	1 038	6
4	$^6H_{7/2}$	Γ_8	1 212	1 208	1 205	3
5	$^6H_{7/2}$	Γ_7	1 212	1 216	1 202	14
6	$^6H_{9/2}$	Γ_6	—	2 251	2 245	6
7	$^6H_{9/2}$	aΓ_8	—	2 369	2 361	8
8	$^6H_{9/2}$	bΓ_8	—	2 423	2 420	3
9	$^6H_{11/2}$	aΓ_8	—	3 641	3 646	−5
10	$^6H_{11/2}$	Γ_7	—	—	3 676	—
11	$^6H_{11/2}$	bΓ_8	—	3 692	3 696	−4
12	$^6H_{11/2}$	Γ_6	—	3 705	3 706	−1
13	$^6H_{13/2}$	aΓ_8	—	5 005	5 013	−8
14	$^6H_{13/2}$	Γ_6	—	(5012)	5 020	−8
15	$^6H_{13/2}$	aΓ_7	—	5 027	5 040	−13
16	$^6H_{13/2}$	bΓ_7	—	5 139	5 136	3
17	$^6H_{13/2}$	bΓ_8	—	5 146	5 161	−15
18	$^6H_{15/2}$	aΓ_8	—	(6285)	6 285	0
19	$^6F_{1/2}$	Γ_6	—	6 355	6 374	−19
20	$^6H_{15/2}$	bΓ_8	—	(6397)	6 392	5
21	$^6F_{3/2}$	Γ_8	—	6 611	6 617	−6
22	$^6H_{15/2}$	Γ_7	—	—	6 630	—
23	$^6H_{15/2}$	cΓ_8	—	(6759)	6 759	0
24	$^6H_{15/2}$	Γ_6	—	—	6 795	—
25	$^6F_{5/2}$	Γ_8	—	7 106	7 113	−7
26	$^6F_{5/2}$	Γ_7	—	7 181	7 189	−8
27	$^6F_{7/2}$	Γ_6	—	—	7 957	—
28	$^6F_{7/2}$	Γ_8	—	7 954	7 958	−4
29	$^6F_{7/2}$	Γ_7	—	8 079	8 091	−12
30	$^6F_{9/2}$	Γ_6	—	9 098	9 081	17
31	$^6F_{9/2}$	aΓ_8	—	9 155	9 153	2
32	$^6F_{9/2}$	bΓ_8	—	9 180	9 190	−10
33	$^6F_{11/2}$	Γ_6	—	10 461	10 459	2
34	$^6F_{11/2}$	aΓ_8	—	10 486	10 490	−4
35	$^6F_{11/2}$	Γ_7	—	10 553	10 561	−8
36	$^6F_{11/2}$	bΓ_8	—	10 596	10 607	−11
37	$(^4G + {}^4F)_{5/2}$	Γ_8	17 738	17 742	17 740	2
38	$(^4G + {}^4F)_{5/2}$	Γ_7	18 082	18 086	18 104	−18
39	$^4F_{3/2}$	Γ_8	18 803	18 793	18 797	−4
40	$(^4G + {}^4F)_{7/2}$	Γ_6	—	19 858	19 821	37
41	$(^4G + {}^4F)_{7/2}$	Γ_8	—	19 954	19 953	1
42	$(^4G + {}^4F)_{7/2}$	Γ_7	—	20 109	20 112	−3
43	$^4I_{9/2} + {}^4M_{15/2}$	Γ_8	—	20 311	20 332	−21
44	$^4I_{9/2} + {}^4M_{15/2}$	Γ_8	—	20 331	20 357	−26
45	$^4I_{9/2} + {}^4M_{15/2}$	Γ_8	—	20 482	20 490	−8
46	$^4I_{9/2}$	Γ_6	—	20 559	20550	9
47	$^4I_{9/2} + {}^4M_{15/2}$	Γ_8	—	20 580	20 569	11
48	$^4M_{15/2}$	Γ_7	—	20 606	20 626	−20
49	$^4I_{11/2} + {}^4M_{15/2}$	Γ_6	20 856	20 858	20 856	2
50	$^4I_{11/2}$	Γ_7	20 936	20 936	20 951	−15

Table 1. (Continued.)

Level no.	Multiplet term[a]	CF level[b]	Obs. [1][c] Denning	Obs. this study[d]	Calc.[e]	Δ[f]
51	$^4I_{11/2} + {}^4M_{15/2}$	Γ_8	—	—	20 952	—
52	$^4I_{11/2} + {}^4M_{15/2}$	Γ_8	21 080	21 082	21 076	6
53	$^4I_{11/2} + {}^4M_{15/2}$	Γ_6	21 114	21 114	21 131	−17
54	$(^4I + {}^4K)_{11/2}$	Γ_8	21 231	(21235)	21 207	28
55	$(^4I + {}^4K)_{13/2}$	Γ_8	(21440)	(21440)	21 441	−1
56	$(^4I + {}^4K)_{13/2}$	Γ_6	(21465)	(21457)	21 443	14
57	$(^4I + {}^4K)_{13/2}$	Γ_7	(21485)	21 487	21 460	27
58	$(^4I + {}^4K)_{13/2}$	Γ_8	21 515	(21509)	21 485	24
59	$(^4I + {}^4K)_{13/2}$	Γ_7	21 515	21 516	21 496	20
60	$(^4F + {}^4G)_{5/2}$	Γ_7	22 034	22 038	22 028	10
61	$(^4F + {}^4G)_{5/2}$	Γ_8	22 095	22 095	22 111	−16
62	$^4M_{17/2}$	Γ_6	(22332)	—	22 355	—
63	$^4M_{17/2}$	Γ_8	(22350)	(22337)	22 362	−25
64	$^4M_{17/2}$	Γ_7	—	(22337)	22 365	−28
65	$^4M_{17/2}$	Γ_8	—	(22355)	22 378	−23
66	$^4G_{9/2} + {}^4M_{17/2}$	Γ_8	22 514	22 520	22 526	−6
67	$^4G_{9/2} + {}^4M_{17/2}$	Γ_6	22 573	(22559)	22 571	−12
68	$(^4I + {}^4M)_{15/2}$	Γ_8	22 700	22 699	22 689	10
69	$^4G_{9/2} + {}^4I_{15/2}$	Γ_8	22 728	22 732	22 741	−9
70	$^4G_{9/2} + {}^4I_{15/2}$	Γ_8	22 859	—	22 834	—
71	$(^4I + {}^4M)_{15/2}$	Γ_7	—	—	22 872	—
72	$^4G_{9/2} + {}^4M_{17/2}$	Γ_6	(22901)	(22905)	22 891	14
73	$^4G_{9/2} + {}^4M_{17/2}$	Γ_8	(22901)	22 915	22 895	20
74	$(^4I + {}^4M)_{15/2}$	Γ_6	—	—	23 088	—
75	$(^4I + {}^4M)_{15/2}$	Γ_8	23 123	23 123	23 109	14
76	$(^6P + {}^4P)_{5/2}$	Γ_7	23 659	23 666	23 678	−12
77	$(^6P + {}^4P)_{5/2}$	Γ_8	23 715	23 720	23 714	6
78	$^4M_{19/2}$	Γ_7	—	(23843)	23 833	10
79	$^4M_{19/2}$	Γ_8	—	23 869	23 856	13
80	$^4M_{19/2}$	Γ_6	—	—	23 887	—
81	$^4M_{19/2}$	Γ_6	—	(23976)	23 977	−1
82	$^4M_{19/2}$	Γ_8	—	—	24 005	—
83	$^4M_{19/2}$	Γ_7	—	—	24259	—
84	$^4M_{19/2}$	Γ_8	—	—	24 266	—
85	$(^4L + {}^4I)_{13/2}$	Γ_7	24 395	24 387	24 406	−19
86	$(^4L + {}^4I)_{13/2}$	Γ_8	24 416	24 424	24 421	3
87	$(^4L + {}^4I)_{13/2}$	Γ_7	24 462	24 467	24 465	2
88	$(^6P + {}^4P)_{3/2}$	Γ_8	24 483	24 489	24 502	−13
89	$(^4L + {}^4I)_{13/2}$	Γ_8	24 538	(24537)	24 522	15
90	$(^4L + {}^4I)_{13/2}$	Γ_6	24 597	—	24 599	—
91	$(^4F + {}^4G)_{7/2}$	Γ_7	24 706	24 711	24 717	−6
92	$^4F_{7/2} + {}^4K_{11/2}$	Γ_6	24 773	24 773	24 792	−19
93	$(^4F + {}^4G)_{7/2}$	Γ_8	—	—	24 796	—
94	$(^4K + {}^4I)_{11/2}$	Γ_8	(25013)	25 010	25 011	−1
95	$(^4K + {}^4I)_{11/2}$	Γ_8	—	—	25 055	—
96	$^4M_{21/2}$	Γ_8	—	—	25 062	—
97	$(^4K + {}^4I)_{11/2}$	Γ_7	—	(25081)	25 093	−12
98	$(^4K + {}^4I)_{11/2}$	Γ_6	(25090)	(25091)	25 095	−4
99	$^4M_{21/2}$	Γ_6	—	—	25 116	—
100	$^4M_{21/2}$	Γ_8	—	25 120	25 120	0

Table 1. (Continued.)

Level no.	Multiplet term[a]	CF level[b]	Obs. [1][c] Denning	Obs. this study[d]	Calc.[e]	Δ[f]
101	$^4M_{21/2}$	Γ_7	—	—	25 302	—
102	$^4M_{21/2}$	Γ_8	—	—	25 313	—
103	$(^4L + {}^4K)_{15/2}$	Γ_6	—	(25404)	25 393	11
104	$(^4L + {}^4K)_{15/2}$	Γ_8	—	25 431	25 416	15
105	$^4L_{15/2}$	Γ_7	—	—	25 455	—
106	$(^4L + {}^4K)_{15/2}$	Γ_8	—	—	25 513	—
107	$^4G_{11/2}$	Γ_6	25 530	(25536)	25 532	4
108	$^4G_{11/2}$	Γ_8	25 586	(25578)	25 573	5
109	$^4G_{11/2}$	Γ_7	25 609	(25618)	25 610	8
110	$(^4L + {}^4K)_{15/2}$	Γ_8	25 642	25 645	25 625	20
111	$^4M_{21/2}$	Γ_7	—	—	25 675	—
112	$^4G_{11/2}$	Γ_8	—	—	25 676	—
113	$^4M_{21/2}$	Γ_8	—	—	25 687	—
114	$(^6P + {}^4D)_{7/2}$	Γ_7	—	26 219	26 235	−16
115	$(^6P + {}^4D)_{7/2}$	Γ_8	26 261	26 263	26 271	−8
116	$(^2P + {}^4D)_{1/2}$	Γ_6	—	(26297)	26 275	22
117	$(^6P + {}^4D)_{7/2}$	Γ_6	26 340	26 345	26 335	10
118	$(^4L + {}^4K)_{17/2}$	Γ_6	(26515)	(26503)	26 492	11
119	$(^4L + {}^4K)_{17/2}$	Γ_8	(26507)	—	26 506	—
120	$(^4L + {}^4K)_{17/2}$	Γ_7	(26604)	(26612)	26 600	12
121	$(^4L + {}^4K)_{17/2}$	Γ_8	—	—	26 610	
122	$(^4L + {}^4K)_{17/2}$	Γ_8	—	—	26 625	
123	$(^4L + {}^4K)_{17/2}$	Γ_6	—	—	26 659	—
124	$(^4L + {}^4K)_{13/2}$	Γ_6	(26732)	—	26 751	—
125	$(^4L + {}^4K)_{13/2}$	Γ_8	26 781	—	26 794	—
126	$(^4L + {}^4K)_{13/2}$	Γ_7	—	—	26 835	—
127	$(^4L + {}^4K)_{13/2}$	Γ_8	26 873	(26873)	26 867	6
128	$(^4L + {}^4K)_{13/2}$	Γ_7	—	(26884)	26 879	5
129	$^4F_{9/2}$	Γ_8	27 116	(27120)	27 101	19
130	$^4F_{9/2} + {}^4D_{3/2}$	Γ_8	27 146	27 158	27 185	−27
131	$(^6P + {}^4D)_{5/2}$	Γ_8	27 305	27 315	27 323	−8
132	$^4F_{9/2}$	Γ_6	27 373	27 386	27 356	30
133	$(^6P + {}^4D)_{5/2}$	Γ_7	27 408	27 415	27 398	17
134	$^4D_{3/2}$	Γ_8	27 419	(27438)	27422	16
135	$^4H_{7/2}$	Γ_6	27 944	27 956	27 963	−7
136	$^4H_{7/2}$	Γ_8	28 083	28 093	28 092	1
137	$^4H_{7/2}$	Γ_7	28 156	28 165	28 139	26
138	$(^4K + {}^4L)_{15/2}$	Γ_7	—	28 539	28 537	2
139	$(^4K + {}^4L)_{15/2}$	Γ_8	—	(28556)	28 565	1
140	$(^4K + {}^4L)_{15/2}$	Γ_6	—	—	28 568	—
141	$(^4K + {}^4L)_{15/2}$	Γ_8	—	(28590)	28 572	18
142	$(^4K + {}^4L)_{15/2}$	Γ_8	—	28 629	28 611	18
143	$^4D_{7/2} + {}^6P_{7/2}$	Γ_7	—	(28660)	28 673	−13
144	$^4H_{9/2}$	Γ_6	—	(28700)	28 708	−8
145	$^4H_{9/2}$	Γ_8	—	28 722	28 732	−10
146	$^4D_{7/2} + {}^6P_{7/2}$	Γ_8	—	—	28 748	—
147	$^4H_{9/2}$	Γ_8	—	28 773	28 777	−4
148	$^4D_{7/2} + {}^6P_{7/2}$	Γ_6	—	—	28 789	—
149	$(^4L + {}^4K)_{17/2}$	Γ_6	—	—	28 900	—
150	$(^4L + {}^4K)_{17/2}$	Γ_8	—	—	28 909	—

Table 1. (Continued.)

Level no.	Multiplet term[a]	CF level[b]	Obs. [1][c] Denning	Obs. this study[d]	Calc.[e]	Δ[f]
151	$(^4L + {}^4K)_{17/2}$	Γ_7	—	—	28 910	—
152	$^4L_{19/2} + {}^4H_{11/2}$	Γ_8	—	—	28 935	—
153	$^4K_{17/2} + {}^4L_{19/2}$	Γ_7	—	—	28 982	—
154	$(^4L + {}^4K)_{17/2}$	Γ_8	—	—	29 003	—
155	$(^4L + {}^4K)_{17/2}$	Γ_8	—	—	29 012	—
156	$(^4L + {}^4K)_{17/2}$	Γ_6	—	—	29 029	—
157	$^4H_{11/2} + {}^4L_{19/2}$	Γ_8	—	29 060	29 062	−2
158	$^4H_{11/2} + {}^4L_{19/2}$	Γ_6	—	—	29 122	—
159–169						
170	$^4H_{13/2}$	Γ_7	—	—	29 493	—
171	$^4G_{7/2}$	Γ_7	—	(29800)	29 804	−4
172	$^4G_{7/2} + {}^4G_{9/2}$	Γ_8	—	(29826)	29 832	−6
173	$^4G_{7/2}$	Γ_6	—	(29844)	29 836	8
174	$^4G_{5/2} + {}^4G_{7/2}$	Γ_8	—	(29893)	29 906	−13
175	$^4G_{9/2}$	Γ_6	—	—	29 942	—
176	$^4G_{9/2}$	Γ_8	—	(29993)	29 983	10
177	$^4G_{5/2} + {}^4G_{9/2}$	Γ_8	—	—	30 124	—
178	$^4G_{5/2}$	Γ_7	—	30 225	30 216	9
179	$^2L_{15/2}$	Γ_8	—	—	30 991	—
180	$(^4P + {}^2P)_{1/2}$	Γ_6	—	31 039	31 019	20
181	$^2L_{15/2}$	Γ_8	—	—	31 111	—
182	$^4G_{11/2} + {}^4P_{3/2}$	Γ_8	—	—	31 151	—
183	$^2L_{15/2} + {}^4G_{11/2}$	Γ_7	—	31 171	31 170	1
184	$^2L_{15/2} + {}^4G_{11/2}$	Γ_7	—	(31233)	31 232	1
185	$^4G_{11/2}$	Γ_6	—	—	31 323	—
186	$^4G_{11/2}$	Γ_8	—	—	31 326	—
187	$^4P_{3/2} + {}^4G_{11/2}$	Γ_8	—	(31451)	31 480	−29
188	$^2L_{15/2}$	Γ_8	—	31 508	31 537	−29
189	$^2L_{15/2}$	Γ_6	—	(31506)	31 542	−36
190	$(^4P + {}^4D)_{5/2}$	Γ_8	—	32 464	32 455	9
191	$(^4P + {}^4D)_{5/2}$	Γ_7	—	32 570	32 563	7
192	$(^4P + {}^2F)_{5/2}$	Γ_8	—	(33308)	33 263	45
193	$^2K_{13/2}$	Γ_6	—	—	33 430	—
194	$^2K_{13/2}$	Γ_7	—	—	33 476	—
195	$^2K_{13/2}$	Γ_8	—	—	33 500	—
196	$(^4F + {}^4G)_{9/2}$	Γ_8	—	(33546)	33 574	−28
197	$(^4F + {}^4G)_{9/2}$	Γ_8	—		33 722	—
198	$^4F_{9/2}$	Γ_6	—	—	33 778	—
199	$^2F_{5/2}$	Γ_7	—	—	33 805	—
200	$^2K_{13/2}$	Γ_8	—	—	33 845	—
201	$^2K_{13/2}$	Γ_7	—	—	33 887	—
202	$^2L_{17/2}$	Γ_7	—	—	34 081	—
203	$^2L_{17/2}$	Γ_8	—	—	34 083	—
204	$^2L_{17/2}$	Γ_8	—	34 099	34 096	3
205	$^4I_{9/2} + {}^2L_{17/2}$	Γ_8	—	—	34 140	—
206	$^2L_{17/2}$	Γ_6	—	—	34 140	—
207	$^2L_{17/2}$	Γ_6	—	—	34 274	—
208	$^2L_{17/2}$	Γ_8	—	34 286	34 281	5
209	$(^4I + {}^4F)_{9/2}$	Γ_8	—	—	34 301	—
210	$(^4I + {}^2F)_{9/2}$	Γ_6	—	—	34 361	—

Table 1. (Continued.)

Level no.	Multiplet term[a]	CF level[b]	Obs. [1][c] Denning	Obs. this study[d]	Calc.[e]	Δ[f]
211–223						
224	$^2I_{11/2}$	Γ_7	—	(35704)	35 702	2
225–237						
238	$^4F_{3/2}$	Γ_8	—	36 386	36 381	−5
239–252						
253	$(^4I + {}^2H)_{9/2}$	Γ_8	—	—	37 271	—
254	$(^4I + {}^2H)_{9/2}$	Γ_8	—	37 295	37 281	14
255	$^2F_{7/2}$	Γ_8	—	—	37 835	—

[a] Only one or two dominant terms are shown. The notation $(^{2S+1}L + {}^{2S'+1}L')_J$ is short for $^{2S+1}L_J + {}^{2S'+1}L'_J$. In regions where no experimental data are available (e.g. levels 159–169) the tabulation of calculated energies has been omitted.
[b] The labels a, b, c . . . for CF levels 1–36 arrange the same irreps within a given multiplet term in ascending order of energy. The eigenvectors of states are very mixed for higher CF levels so that these labels a, b, c . . . are then omitted.
[c] Observed energy from the TPE study of $Cs_2NaYCl_6:Sm^{3+}$ in [1]. The level assignments have been changed from those in [1] in some cases, as shown in table 3.
[d] Observed energy from the absorption spectrum of $Cs_2NaSmCl_6$. Uncertain assignments are in parentheses. An experimental Γ_6 level at 7957 cm^{-1} was not included in the energy level fittings.
[e] The $4f^5 + 4f^46p$ CIACF calculation.
[f] Δ is the difference between the observed and calculated energies of $Cs_2NaSmCl_6$.

the following. Although the first two $^{2S+1}L_J$ eigenvector components of excited crystal field states are listed in some cases in table 1, for conciseness only the first component is usually referred to in the following.

3.1. Transitions to ^6H_J ($2J = 7, 9, 11, 13, 15$) (levels 1–24, excluding 19, 21)

The first problematic energy level assignment is for the excited multiplet term, $^6H_{7/2}$, near 1000 cm^{-1}, which comprises the Γ_6, Γ_7 and Γ_8 CF levels. These levels were assigned in order of increasing energy Γ_6, Γ_7, Γ_8 by Banerjee and Schwarz, but the Γ_7 level was then reassigned to be above Γ_8 [4, 5, 27], and at the same energy as Γ_8 [1] in subsequent studies. The rationale in the assignment of the $(^4G_{5/2})\Gamma_8 \rightarrow {}^6H_{7/2}$ emission study of $Cs_2NaYCl_6:Sm^{3+}$ [5] was that three intense bands were observed and assigned to the three expected MD origins. It is clear that the stronger two bands correspond to $\Gamma_8 \rightarrow \Gamma_6$, $\Gamma_8(^6H_{7/2})$ since these MD transitions are calculated to be strong, and of similar intensity. The $\Gamma_8 \rightarrow \Gamma_7$ transition was calculated to be weaker, and was therefore assigned to one shoulder at 6 cm^{-1} to low energy of the $(^4G_{5/2})$ $\Gamma_8 \rightarrow \Gamma_8$ transition. The energies of the $(^6H_{7/2})$ Γ_6, Γ_8, Γ_7 levels in $Cs_2NaYCl_6:Sm^{3+}$ are then (in cm^{-1}) 1045, 1210, 1216 cm^{-1}.

The room temperature and 90 K absorption spectra in the region of the $^6H_{5/2} \rightarrow {}^6H_{7/2}$ transition of $Cs_2NaSmCl_6$ were recorded. The most intense bands correspond to MD allowed transitions and the calculated relative intensities of these bands are in satisfactory agreement with experiment. The energies of the $^6H_{7/2}$ CF levels in $Cs_2NaSmCl_6$ are then within 2 cm^{-1} of the derived values from the emission spectrum of $Cs_2NaYCl_6:Sm^{3+}$ [5].

The $^6H_{9/2}$ levels are assigned from weak ZPLs in the 90 K absorption spectrum, in agreement with the derived energies from emission spectra [5]. Three of the four congested $^6H_{11/2}$ levels can be assigned from the absorption spectrum, with an intense MD origin corresponding to the $\Gamma_7 \rightarrow b\Gamma_8$ transition. The oscillator strengths ($\times 10^{-10}$) of the pure electronic transitions from $(^6H_{5/2})\Gamma_7$ to the terminal $a\Gamma_8$, $a\Gamma_7$ and $b\Gamma_7(^6H_{13/2})$ levels are

measured (calculated) as 5.9 (13.1), 6.3 (5.9) and 8.5 (6.8), and associated vibronic structure is observed for these transitions. The transition to $\Gamma_6(^6H_{13/2})$ is MD forbidden. The transition to the bΓ_8 level is calculated to be about 12 times weaker than that to bΓ_7, and is assigned to a sharp, weak band which is otherwise unassigned. The associated ν_3 and ν_4 vibronic origins are also weak. Transitions to $^6H_{15/2}$ cannot be securely assigned since they are hidden in the vibronic structure of transitions to ^6F_J. Some levels are tentatively assigned at 6285 cm^{-1} (from ν_3, ν_4 and ν_6 structure) and at 6759 cm^{-1} (from ν_3 and ν_6 structure), but these vibronic structures all overlap other bands.

3.2. Transitions to ^6F_J ($2J = 1, 3, 5, 7, 9, 11$) (levels 19, 21, 25–36)

These transitions are well-resolved so that the rich vibronic structure is readily assigned. The locations of the ZPLs are marked in figures 1(a), (b). Generally the $\Gamma_7 \rightarrow \Gamma_7 + \nu_6$ transitions are much weaker than $\Gamma_7 \rightarrow \Gamma_7 + (\nu_3$ or $\nu_4)$. By contrast, the $\Gamma_7 \rightarrow (\Gamma_6$ or $\Gamma_8) + \nu_6$ transitions are stronger than $\Gamma_7 \rightarrow (\Gamma_6$ or $\Gamma_8) + (\nu_3$ or $\nu_4)$. All of the electronic origins are clearly observed except for the MD forbidden transition $\Gamma_7 \rightarrow \Gamma_6(^6F_{7/2})$. At 60 K a hot band is observed at 7792 cm^{-1} for which most of the MD intensity is calculated to come from $\Gamma_8 \rightarrow \Gamma_6(^6F_{7/2})$, so that the Γ_6 level is tentatively inferred to be at 7957 cm^{-1} (and not included in table 1), which is very near to the energy of Γ_8.

3.3. Transitions to $(^4G + ^4F)_J$ ($2J = 5, 7$) and $^4F_{3/2}$ in the region 17 700–20 200 cm^{-1} (levels 37–42)

The transition $^6H_{5/2} \rightarrow (^4G + ^4F)_{5/2}$ of $Cs_2NaSmCl_6$ is mainly MD in character. Two intense ZPLs are observed, with $\Gamma_7 \rightarrow \Gamma_8$ located at 17 744 cm^{-1} at 60 K, but split into two components at 17 744, 17 739 cm^{-1} at 10 K. The corresponding ZPL is even split by 3 cm^{-1} in the 10 K absorption spectrum of $Cs_2NaY_{0.9}Sm_{0.1}Cl_6$. For $Cs_2NaSmCl_6$ at 60 K, the calculated magnetic dipole intensity ratios, $I(\Gamma_7 \rightarrow \Gamma_8)/I(\Gamma_8 \rightarrow \Gamma_8)$ and $I(\Gamma_7 \rightarrow \Gamma_7)/I(\Gamma_8 \rightarrow \Gamma_7)$, are in agreement with values from [4] and [2], and are also in reasonable agreement with experiment. The $(^6H_{5/2})\Gamma_7 \rightarrow \Gamma_8(^4F_{3/2})$ transition (18 793–19 076 cm^{-1}) is weaker but well-resolved. It is dominated by the ZPL and the ν_6 vibronic origin, with ν_4 very weak.

Finally, the transitions to $(^4G + ^4F)_{7/2}$ lie between 19 858 and 20 360 cm^{-1} at 10 K. The assignment of level 40 exhibits a large discrepancy with calculation. A weak ZPL is observed at 19 858 cm^{-1}, corresponding to $\Gamma_7 \rightarrow \Gamma_6(^4G + ^4F)_{7/2}$. The associated ν_6 vibronic origin is observed at 10 K, as well as the sharp ZPL $\Gamma_8 \rightarrow \Gamma_6$ (19 693 cm^{-1}) at 60 K. The discrepancy of the $4f^5$ calculation energy (19 802 cm^{-1}) and the $4f^5 + 4f^4 6p$ calculation energy (19 821 cm^{-1}) from the observed energy of level 40 is not due to a resonance of the electronic and vibronic levels of the type that has been found in $Cs_2NaLnCl_6$ (Ln = Tm, Yb) because in this case it is the lower energy state that is anomalous in energy.

The next-highest level (41: $(^4G + ^4F)_{7/2}\Gamma_8$) has an intense ZPL at 19 954 cm^{-1}. In fact, both of the $\Gamma_7 \rightarrow \Gamma_8$, Γ_7 $(^4G + ^4F)_{7/2}$ transitions are clearly assigned from the MD electronic origins and the associated vibronic structure, but at rather different energies from those of Foster *et al* [4], which were at 19 972, 20 130 cm^{-1}.

3.4. Transitions to $^4M_{15/2}$ and $^4I_{9/2}$ in the region 20 311–20 857 cm^{-1} (levels 43–48)

The energy levels are of notably mixed SLJ-parentage above 20 300 cm^{-1}, with the major components of those between 20 311–20 606 cm^{-1} being $^4I_{9/2}$ and $^4M_{15/2}$. Thorne *et al* [1] were unable to investigate the TPE spectra in this region, and included two levels from [2],

located at 20 389 and 20 553 cm^{-1}, in their energy level fit. Our assignments serve to confirm the second, but not the first, of these levels.

Two medium intensity, sharp bands are observed at 20 311 and 20 331 cm^{-1}, and the observation of associated vibronic structure at 10 K, and hot bands at 60 K, serves to confirm their assignments to electronic origins. The two states calculated to be at considerably lower energy in this region are two $(^4I_{9/2} + {}^4M_{15/2})\Gamma_8$ states. From the analysis of ZPL and vibronic structure, further levels are clearly identified at 20 482, 20 559 and 20 606 cm^{-1}. A further transition may be less conclusively assigned at 20 580 cm^{-1}, but all spectral features in this region are clearly accounted for and there is a one-to-one mapping of observed energy levels with calculation.

3.5. Transitions to ^4I_J ($2J = 11, 13$), $^4M_{15/2}$, $^4K_{13/2}$ in the region 20 858–21 796 cm^{-1} (levels 49–59)

The transitions in this region, shown in figure 1(c), mainly terminate upon the ^4I_J ($2J = 11, 13$) multiplet terms which are mixed with $^4M_{15/2}$ and $^4K_{13/2}$, respectively. Six terminal states are clearly located, and a further four states are tentatively located in this region in order to account for all features. The energies of the CF levels are similar to those in [1] (refer to table 1). Levels 55 and 56 are calculated to be close in energy. Our listing in table 1 follows, without further evidence, the same order as the calculation (i.e. $\Gamma_8 < \Gamma_6$), which is the reverse order of [1]. Much closer agreement with calculation could be obtained by deleting our tentative assignment of level 58 and moving levels 54–57 inclusive up by one place but we have not done this.

3.6. Transitions to states involving $^4F_{5/2}$, ^4G_J, ($2J = 5, 9$), ^4M_J ($2J = 15, 17$), $^4I_{15/2}$ in the region 22 038–23 403 cm^{-1} (levels 60–75)

This spectral region is also very congested. At the beginning of this spectral region, figure 1(d), two intense MD ZPLs, associated with the terminal CF levels of $(^4F + {}^4G)_{5/2}$, are observed (in cm^{-1}) at 22 038 (literature values 22 055 [4], 22 046 [2]) and 22 095 (literature values 22 112 [4], 22 091 [2]), with weak vibronic structure to high energy. A further prominent ZPL is observed at 22 337 cm^{-1}. The terminal state(s) correspond(s) to the $(^4M_{17/2})\Gamma_8$ and/or Γ_7 (but not Γ_6) level tentatively assigned at similar energy from the TPE study. At 60 K, the pure electronic transitions to these three levels from $(^6H_{5/2})\Gamma_8$ are observed. Further sharp ZPLs are observed (in cm^{-1}) at 22 520, 22 699, 22 732 (literature 22 766 [2]) and 22 915, with associated vibronic sidebands to higher energy. At highest energy the weak vibronic sideband of an electronic origin inferred to be at 23 123 cm^{-1} is observed. Further transitions to levels tentatively located at 22 355 and 22 559 cm^{-1} account for all observed features.

3.7. Transitions to states involving $(^6P + {}^4P)_J$ ($2J = 3, 5$), ^4L_J ($2J = 13, 15$), $^4F_{7/2}$, ^4K_J ($2J = 11, 15$), ^4I_J ($2J = 11, 13$), ^4G_J ($2J = 7, 11$), ^4M_J ($2J = 19, 21$) in the region 23 666–25 930 cm^{-1} (levels 76–113)

Four main groups of bands are observed in this region, and the transitions are mainly vibronic in character. The first group, between 23 666 and 24 105 cm^{-1}, is dominated by the vibronic structure of transitions to the two $(^6P + {}^4P)_{5/2}$ CF levels. Further electronic origins are inferred to be at 23 720 and 23 869 cm^{-1} from characteristic vibronic structures. The remaining bands can be assigned in several ways, one of which infers further electronic origins to be at 23 843 and 23 976 cm^{-1}.

For the second group, four transitions, each with vibronic structure, are resolved between 24 387 and 25 058 cm^{-1}. Consistent with these, four weak hot bands at 60 K are assigned to

Table 2. $(^6H_{5/2})\Gamma_7 \rightarrow \Gamma_7(^6P_{7/2} + {}^4D_{7/2})$ absorption spectrum of $Cs_2NaSmCl_6$. (Note: The energies of the $^6H_{5/2}\Gamma_7$ and $\Gamma_7(^6P_{7/2} + {}^4D_{7/2})$ states are 0 and 26 219 cm^{-1}, respectively. The line marked −1 in figure 1(e)(ii) corresponds to the $(^6H_{5/2})\Gamma_7 + \nu_6 \rightarrow \Gamma_8(^6P_{7/2} + {}^4D_{7/2})$ transition.)

		Assignment and derived vibrational energy	
Line figure 1(e) (i), (ii)	Energy (cm^{-1})	Initial state, $^6H_{5/2}$	Terminal state, $^6P_{7/2}$
−2	26 119	$\Gamma_7 + S_7$ (100)	Γ_7
0	26 219	Γ_7	Γ_7
1	26 258	Γ_7	$\Gamma_7 + S_5(39)$
2	26 278	Γ_7	$\Gamma_7 + S_9(59)$
3	26 291	Γ_7	$\Gamma_7 + S_{10}(72)$
4	26 302	Γ_7	$\Gamma_7 + S_{10}(83)$
5	26 317	Γ_7	$\Gamma_7 + S_7(98)$
6	26 340	Γ_7	$\Gamma_7 + S_7(121)$
7	26 457	Γ_7	$\Gamma_7 + S_6(238)$
8	26 471	Γ_7	$\Gamma_7 + S_6(252)$
9	26 503	Γ_7	$\Gamma_7 + S_6(284)$

the $\Gamma_8 \rightarrow \Gamma_7, \Gamma_8$, $\Gamma_7(^4L + {}^4I)_{13/2}$ and $\Gamma_8 \rightarrow \Gamma_8(^6P + {}^4P)_{3/2}$ electronic origins. The assignment of weaker bands in this region is not as straightforward. A further origin is tentatively assigned at 24 537 cm^{-1} from ν_3 and ν_4 structure. Unobserved origins can be assigned at 24 711 and 24 773 cm^{-1} on the basis of the associated ν_3, ν_4 and ν_6 vibronic origins.

For the third group, between 25 010 and 25 408 cm^{-1}, the assignments are tentative but again account for all bands. A ZPL is located at 25 010 cm^{-1}, together with ν_3, ν_4 and ν_6 vibronic origins to higher energy. The remaining weak vibronic structure can be assigned to terminal levels at 24 711, 25 081, 25 091 and 25 120 cm^{-1}.

A further complex, weak group of bands is observed between 25 431 and 25 930 cm^{-1}. The transitions at 25 431 and 25 645 cm^{-1} can be assigned with certainty. All of the remaining bands can be assigned to structure based upon a further four electronic origins. The irreps of the CF levels are then assigned by reference to the calculation.

3.8. Transitions to levels involving ^6P_J ($2J = 5, 7$), $^4D_{3/2}$, ^4L_J ($2J = 13, 17$), $^4F_{9/2}$ in the region 26 219–27 800 cm^{-1} (levels 114–134)

This region consists of two main groups of bands, from 26 219 to 26 760 cm^{-1}, and from 27 127 to 27 670 cm^{-1}. The first group is shown in figure 1(e)(i), with a ZPL at 26 219 cm^{-1} (marked 0) and complete associated vibronic structure (assigned in table 2) to higher energy. The figure also shows the 10 K spectrum of $Cs_2NaYCl_6:Sm^{3+}$ (figure 1(e)(iii)) where the ZPL only shifts about 10 cm^{-1} to low energy. Thus by contrast to the TPE spectrum, where the lowest $(^6P + {}^4D)_{7/2}$ level, Γ_7, was assigned at 26 261 cm^{-1}, it is clearly assigned at 26 219 cm^{-1} in $Cs_2NaSmCl_6$ herein. Figure 1(e)(ii) also shows the 60 K hot band at 26 119 cm^{-1}($\Gamma_7 + \nu_4 \rightarrow \Gamma_7(^6P + {}^4D)_{7/2}$: marked −2 in the figure). By contrast, the vibronic structure upon the next-highest transition, with an (unobserved) electronic origin inferred to be at 26 263 cm^{-1}, is much weaker but clearly identified from the ν_6 vibronic origin and associated ν_6 hot band (marked −1 in figure 1(e)(ii)), as well as other vibronic structure. The irrep assigned to this level (Γ_8) thus differs from that in [1] (Γ_7). Other transitions in this region can be assigned to terminal levels at 26 297 cm^{-1} (116), 26 345 cm^{-1} (117), and tentatively at 26 503 cm^{-1} (118) and 26 612 cm^{-1} (120 or 121) to account for all of the structure in figure 1(e) and the locations of the (inferred) ZPLs are marked.

The next-highest energy group of bands has two ZPLs at 27 120 and 27 158 cm^{-1} and extensive vibronic structure is resolved for the latter but not for the former. A further three electronic transitions can be confidently assigned, and two tentatively assigned, with only one weak band at 27 536 cm^{-1} remaining unassigned. This is most reasonably assigned to the ν_4 vibronic origin of a ZPL inferred to be at 27 438 cm^{-1}. There is a systematic error of $\sim$10 cm^{-1} in this region with the levels reported by Thorne *et al*, part of which is probably due to calibration uncertainties.

3.9. Transitions to states containing ^4H_J ($2J = 7, 9$), $^4K_{15/2}$, $^4L_{15/2}$, $^4D_{7/2}$, $^6P_{7/2}$ in the region 27 955–29 058 cm^{-1} (levels 135–148)

The first transition in this region is dominated by intense MD ZPLs at 28 093 and 28 165 cm^{-1} and this aids the assignment to the $\Delta J = 1$ transitions $(^6H_{5/2})\Gamma_7 \rightarrow \Gamma_8, \Gamma_7$ $(^4H_{7/2})$. To low energy, the weak ν_4 and stronger ν_6 vibronic structure of the $\Gamma_7 \rightarrow \Gamma_6$ $(^4H_{7/2})$ transition is observed. The MD forbidden $\Gamma_7 \rightarrow \Gamma_6$ origin is not observed but the $\Gamma_8 \rightarrow \Gamma_6$ transition is observed at 27 794 cm^{-1} at 60 K. The next group of bands is from 28 539 to 29 058 cm^{-1}. At low energy, ZPLs are located at 28 539 and 28 629 cm^{-1}, with extensive vibronic structure. Strong vibronic origins are also observed, based upon ZPLs inferred to be at 28 722 and 28 773 cm^{-1}. The further assignments in this region are tentative but account for all observed bands.

3.10. Transitions in the region above 29 730 cm^{-1} (levels 174–254)

In this region some transitions can be clearly identified from their vibronic structure, but the assignment to specific representations is purely based upon the calculation. Our spectra are not as clearly resolved as in the infrared spectral region as typified by the region between 31 000 and 31 800 cm^{-1} shown in figure 1(f), where the inferred locations of electronic origins are marked. The absorbance increases above 38 000 cm^{-1} and there is total absorption at 39 000 cm^{-1}.

3.11. Comparison with two-photon excitation (TPE) study

Energy levels deduced from the polarized TPE study of Cs_2NaYCl_6:Sm^{3+} by Thorne *et al* are also included in table 1, column 4, although the assignments in some cases have been changed, as shown in table 3. In principle, the TPE experiments enable the assignment of peaks to terminal states of Γ_7/Γ_8 or Γ_6/Γ_8 irreps [1]. Thus the interchanges of Γ_6/Γ_8 irreps for 55/56, 72, 92/93 and 99/100, 115, 125, or Γ_7/Γ_8 irreps for level 73, are not contrary to the TPE results. Likewise, 26 261 cm^{-1} was identified as level 114 and assigned as Γ_7 in [1], while in this study 26 263 cm^{-1} is assigned as level 115 (Γ_8) and 26 219 cm^{-1} (not observed in [1]) fills the gap as 114 (Γ_7). Elsewhere, a given TPE energy has been reassigned to the same irrep, but a different number level with different multiplet term (i.e. for TPE energies 25 642 cm^{-1} (level 110 herein) and (26732) cm^{-1} (124)). However, for some other cases (levels 71, 132, 133) the irrep or the assignment energy has been changed from that in [1]: $\Gamma_6 \leftrightarrow \Gamma_7$ and such a distinction should be contrary to the TPE results. In part, this could be due to the crystal imperfections and optical alignment, and also to the deviation of the crystal from cubic symmetry. Thus, for example, the strong transition to 117 ($\Gamma_7 \rightarrow \Gamma_6$, TPE energy 26 340 cm^{-1} in [1], also transition 117 herein) is actually forbidden in the 0° polarization (figure 3(c) of [1]) but is the strongest feature in that spectral region. In another case, transition 133 in [1] was assigned to $\Gamma_7 \rightarrow \Gamma_6$ because it shows a slight increase in intensity in the 45° polarization, but this is probably due to the overlapping $\Gamma_7 \rightarrow \Gamma_8$ transition. The intensities in the region between 20 800 and 21 800 cm^{-1} in the TPE spectrum are distorted by resonance enhancement by absorption into $^6F_{11/2}$. The starred bands in figure 2(a) of [1] can all be assigned to excited state absorption (odd-phonon) vibronic intervals of 84, 108, 186 and 251 cm^{-1} based upon the CF levels of $^6F_{11/2}$.

Table 3. Energy level notations and assignments in this study which differ from those of [1].

	This study			Reference [1]		
Level no.	Multiplet term	CF level	Obs.	Multiplet term	CF level	Obs.
55	$(^4I + {}^4K)_{13/2}$	Γ_8	(21440)	$^4I_{13/2}$	Γ_8	(21465)
56	$(^4I + {}^4K)_{13/2}$	Γ_6	(21457)	$^4I_{13/2}$	Γ_6	(21440)
60	$(^4F + {}^4G)_{5/2}$	Γ_7	22 038	$^4F_{5/2}$	Γ_6	22 034
71	$(^4I + {}^4M)_{15/2}$	Γ_7	—	$^4M_{17/2}$	Γ_6	—
72	$^4G_{9/2} + {}^4M_{17/2}$	Γ_6	(22905)	$^4I_{15/2}$	Γ_8	(22901)
73	$^4G_{9/2} + {}^4M_{17/2}$	Γ_8	22 915	$^4I_{15/2}$	Γ_7	(22901)
92	$^4F_{7/2} + {}^4K_{11/2}$	Γ_6	24 773	$^4F_{7/2}$	Γ_8	24 773
93	$(^4F + {}^4G)_{7/2}$	Γ_8	—	$^4F_{7/2}$	Γ_6	—
95	$^4K_{11/2}$	Γ_8	—	$^4M_{21/2}$	Γ_8	—
96	$^4M_{21/2}$	Γ_8	(25081)	$^4K_{11/2}$	Γ_8	—
97	$(^4K + {}^4I)_{11/2}$	Γ_7	—	$^4M_{21/2}$	Γ_7	—
99	$^4M_{21/2}$	Γ_6	—	$^4M_{21/2}$	Γ_8	—
100	$^4M_{21/2}$	Γ_8	25 120	$^4K_{11/2}$	Γ_6	(25090)
110	$(^4L + {}^4K)_{15/2}$	Γ_8	25 645	$^4G_{11/2}$	Γ_8	25 642
112	$^4G_{11/2}$	Γ_8	—	$^4M_{21/2}$	Γ_8	—
113	$^4M_{21/2}$	Γ_8	—	$^4G_{11/2}$	Γ_8	25 642
114	$(^6P + {}^4D)_{7/2}$	Γ_7	26 219	$^4P_{7/2}$	Γ_7	26 261
115	$(^6P + {}^4D)_{7/2}$	Γ_8	26 263	$^4D_{1/2}$	Γ_6	—
124	$(^4L + {}^4K)_{13/2}$	Γ_6	—	$^4L_{17/2}$	Γ_6	26 732
125	$(^4L + {}^4K)_{13/2}$	Γ_8	—	$^4K_{13/2}$	Γ_6	26 781
132	$^4F_{9/2}$	Γ_6	27 386	$^4D_{5/2}$	Γ_7	27 373
133	$(^6P + {}^4D)_{5/2}$	Γ_7	27 415	$^4F_{9/2}$	Γ_6	27 408

3.12. Hypersensitive transitions of Sm^{3+} in $Cs_2NaSmCl_6$

The formal selection rule for hypersensitive transitions $|\Delta J| = 2$ [29] is that for pure electric quadrupole transitions $|\Delta J| \leqslant 2$, $|\Delta L| \leqslant 2$, $\Delta S = 0$ [30]. As mentioned in the introduction there has been some confusion in the literature concerning the nature of the intensity change for hypersensitive transitions when the symmetry of the lanthanide ion is decreased. This is because spectra were taken at low resolution, or were not well-resolved, so that spectral features comprised bands due to both pure electronic transitions and their associated vibronic sidebands. At first, the large intensity of hypersensitive transitions was envisaged to be due to a purely electronic mechanism (e.g. [31, 32]). Later, Judd realized that the vibronic contribution to the intensity of hypersensitive transitions was appreciable [33] and provided a calculation for comparison with the vibronic intensity model of Faulkner and Richardson [34].

Several of the transitions investigated in the present absorption spectral study are hypersensitive and they are all characterized by large vibronic oscillator strengths. For example, the measured oscillator strength of the vibronic sideband of the transition $(^6H_{5/2})\Gamma_7 \rightarrow \Gamma_6(^6F_{1/2})$ in $Cs_2NaSmCl_6$ is $(1.44 \pm 0.07) \times 10^{-7}$. The oscillator strength of the ZPL measured at 300 K was reported to be 2.0×10^{-10} [2] whereas the calculated value for this pure electric quadrupole transition is 2.3×10^{-10} [19]. This oscillator strength is measured to be an order of magnitude greater at 10 K: between (2.9–4.6) $\times 10^{-9}$, depending upon the crystal (refer to line 3 in the lower spectrum of figure 2). This is attributed not only to the introduction of MD character into the transition at temperatures below the phase transition, but also to the effects of crystal strain which introduce noncentrosymmetry at the Sm^{3+} site. The latter consequently

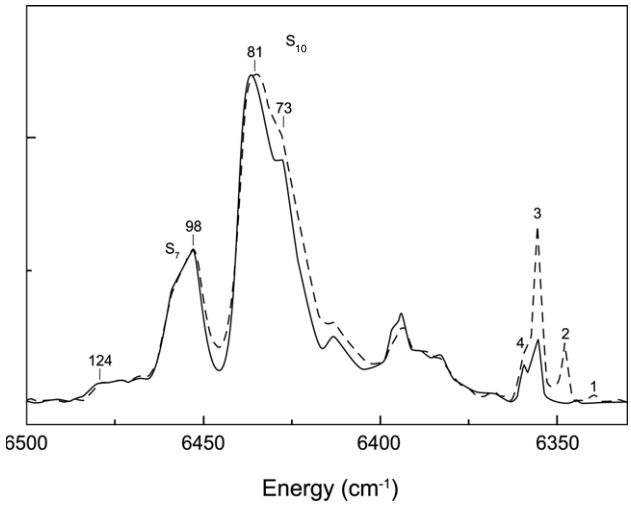

Figure 2. 10 K absorption spectrum in the region of the lower part of the $(^6H_{5/2})\Gamma_7 \rightarrow \Gamma_6(^6F_{1/2})$ hypersensitive transition. The ordinate is absorbance. Lower spectrum: $Cs_2NaSmCl_6$. Upper spectrum: $Cs_2NaSm(Cl_{0.96}Br_{0.04})_6$. Refer to the text for a discussion of the numbered bands. The marked energies (in cm^{-1}) are the vibrational displacements from the electric quadrupole origin.

introduces ED intensity into the transition at the defect site(s) which may be unshifted in energy from the EQ origin. In fact, at 10 K there are two lines (3 and 4, figure 2) near the inferred location (6355 ± 1 cm^{-1}) of the EQ origin from vibronic analysis at (in cm^{-1}): 6346 (0.19), 6356 (1.0), where the numbers in brackets refer to their relative integrated areas. Notice a similar lineshape for the $(^6H_{5/2})\Gamma_7 \rightarrow \Gamma_7(^6P_{7/2})$ electronic origin at 10 K in figure 1(e), line 0.

The $(^6H_{5/2})\Gamma_7 \rightarrow \Gamma_6(^6F_{1/2})$ transition was also investigated in samples where bromide ions replaced chloride in the crystal. In the range of doping, the replacement of only one of the six chloride neighbours of Sm^{3+} mainly occurred so that the site symmetry of Sm^{3+} was lowered to C_{4v} in $SmBrCl_5^{3-}$. The more likely scenario was the replacement of one of the chloride ions in the neighbouring $SmCl_6^{3-}$ ions. This more distant perturbation also lowers the site symmetry to C_{4v}. A typical spectrum of this hypersensitive transition for $Cs_2NaSm(Cl_{1-z}Br_z)_6$ is shown in figure 2 as the upper spectrum, and is normalized to the same intensity of vibronic structure as in $Cs_2NaSmCl_6$. No clear relationship between the total vibronic oscillator strength of this transition and bromide concentration was found from our experiments. Instead, we focus upon the four features observed in the vicinity of the electronic origin. All of these features exhibit increasing oscillator strengths with increasing bromide concentration. Furthermore, the ratio of the intensity of each of these features to that of the vibronic sideband also increases, as is clear from figure 2. The band marked 4 in figure 2 (6359 cm^{-1}: at higher energy than the EQ origin) shows a fairly similar concentration-intensity dependence with the EQ origin (6355 cm^{-1}: band 3) and is also presumably perturbed by $SmCl_5Br^{3-}$ nearest neighbours. The new next-lower energy band (6347 cm^{-1}: band 2) shows a more dramatic intensity increase. Since the ratio of its intensity, relative to that of the 6355 cm^{-1} band, increases linearly with concentration it is associated with the ZPL of the $SmCl_5Br^{3-}$ species. The fourth band (6339 cm^{-1}: band 1) is relatively much weaker.

In conclusion it is clear that the removal of centrosymmetry in the hypersensitive $(^6H_{5/2})\Gamma_7 \rightarrow \Gamma_6(^6F_{1/2})$ transition leads to an increase in the relative intensity of the ZPL compared with that of the electric dipole vibronic sideband.

4. Crystal field calculation—CIACF (configuration interaction assisted crystal field)

The electronic structure of $Cs_2NaSmCl_6$ was determined by solving the secular matrix containing all the usually considered interactions on two bases consisting for one of them: (a) of all the $4f^5|slm_sm_l\rangle$ states; and for the other one: (b) of all the $4f^5|slm_sm_l\rangle$ states with, in addition, all those of the same parity excited configuration $4f^46p^1$. The pertinence of the second operation in the case of the chloroelpasolites $Cs_2NaLnCl_6$ with Ln = Pr^{3+} and Nd^{3+} was shown in [15, 17]. The mean deviations of the CF fitting were reduced from 32.7 to 11.6 cm^{-1} for Pr^{3+} and from 32.2 to 12.9 cm^{-1} for Nd^{3+}.

4.1. Choice of the parameters

Calculations (a) and (b) were carried out utilizing the computer program ATOME dealing with atomic orbitals $|slm_sm_l\rangle$ [17, 35] instead of the widely utilized coupled states $|SLJM_J\rangle$. Scalar, one- two- and three-electron interactions were introduced into the interaction matrix with their usual parameters, i.e. for $4f^5$: the mean energy of the configuration, E_{AVE}; the electrostatic interaction, (F^2, F^4, F^6); the spin–orbit interaction, ζ_f; the electrostatic interconfiguration interaction, (α, β, γ); the magnetic interactions, (M^k, $k = 0(2, 4)$ with $M^2 = 0.56\ M^0$, $M^4 = 0.31\ M^0$; P^k, $k = 2(4, 6)$ with $P^4 = 0.50\ P^2$, $P^6 = 0.10\ P^2$); the three-electron interaction, (T^i, $i = 2, 3, 4, 6, 7, 8$). The crystal field interaction at a cubic symmetry site is written in the Wybourne notation:

$$B_0^4(\mathrm{ff})[(C_0^4 + (5/14)^{1/2}(C_{-4}^4 + C_4^4)] + B_0^6(\mathrm{ff})[C_0^6 - (7/2)^{1/2}(C_{-4}^6 + C_4^6)],$$

with parameters B_0^4(ff) and B_0^6(ff) (with $B_4^4(\mathrm{ff}) = \pm B_0^4(\mathrm{ff})(5/14)^{1/2}$, $B_4^6 = \mp B_0^6(\mathrm{ff})(7/2)^{1/2}$). Hence the total number of parameters is equal to 18.

According to our previous observations on Pr^{3+} and Nd^{3+}, we have assumed that the specific interaction added in priority is the one connecting $4f^5$ and $4f^46p$. Four additional parameters are then required to define the $4f^46p$ excited configuration: (i) ζ_p, the spin–orbit coupling parameter of the p-electron; (ii) ΔE_{AVE}, the energy difference between the barycentres of the two configurations; (iii) the atomic interconfiguration parameters: R^k(f, f, f, p), ($k = 2, 4$); and (iv) B_0^4(fp), ruling the CF interaction between orbitals of both configurations. The parameters ζ_p and ΔE_{AVE} are delivered by Cowan's program RCN31 [36] (being 4567 and 138 729 cm^{-1}, respectively) and are kept fixed. The R^k(f, f, f, p)s from RCN31 (-4252 and -2401 cm^{-1} for $k = 2$ and 4 respectively) are scaled by X, a common multiplier. The two parameters X and B_0^4(fp) are fitted. The total number of parameters is then equal to 20, which is two more than for $4f^5$ and not very penalizing for so many experimental levels.

The dimension of the $4f^5$ matrix is 2002 and it contains 73 terms whereas that of the matrix including both $4f^5$ and $4f^46p$ is equal to $2002 + 6006 = 8008$.

4.2. Energy level fittings in $4f^5$ and $4f^5 + 4f^46p$

Two energy level fits were thus performed utilizing the 135 experimentally observed levels ranging up to 37 295 cm^{-1}. All the measured energy levels were introduced in the $4f^5$ (normal) and $4f^5 + 4f^46p$ fittings. The final mean deviations were equal to 16.9 and 14.5 cm^{-1} in $4f^5$ and $4f^5 + 4f^46p$, respectively. The improvement of the fitting by configuration interaction is quite modest: only 14%. In [1] the standard deviation in $4f^5$ was 16.8 cm^{-1} for 67 levels, which is close to the $4f^5$ value obtained for 135 levels in the present work. The experimental and calculated energies from the present study are listed in table 1, columns 5 and 6, respectively and the corresponding parameters are given in table 4. In table 1 the uncertain energies are between parentheses. Column 3 indicates the irreducible representations and column 4 reports

Table 4. Empirical Hamiltonian parameters of Sm^{3+} in $Cs_2NaSmCl_6$. (Note: N number of levels fitted; n_p number of parameters; σ mean deviation. Parameters in square brackets were held constant.)

Parameter	$4f^5$ CF fit	$4f^5 + 4f^46p^1$ CIACF fit
F^2	78 165	78 159
F^4	56 612	56 763
F^6	40 172	40 206
α	21.70	21.79
β	−717	−739
γ	1564	1571
T^2	256	261
T^3	26	30
T^4	22	34
T^6	−141	−146
T^7	246	266
T^8	382	384
M^0	2.13	2.16
P^2	260	254
ζ_f	1165	1166
B_0^4 (ff)	1855	2293
B_0^6 (ff)	260	369
ΔE_{AVE}	—	[138729]
X	—	0.822
ζ_p	—	[4567]
B_0^4 (fp)	—	17 600
N	135	135
n_p	18	20
σ	16.9	14.5

previously determined energies in Cs_2NaYCl_6:Sm^{3+} from two-photon spectroscopy [1]. A maximum of two leading eigenvector components is given in column 2, but the complete wavevectors contain a larger number of minor components. The symmetry assignments, as compared with [1], were discussed in section 3.11. Up to level 49, the $^{2S+1}L_J$ label assignments are the same in table 1 as in [1]. Levels 50 and 51 are close together and have been interchanged in energy. Other changes in multiplet term parentages are listed in table 3, and include the changes from $^4M_{17/2}$ to $(^4I + {}^4M)_{15/2}$ for 71; from $^4I_{15/2}$ to $(^4G_{9/2} + {}^4M_{17/2})$ for levels 72 and 73; interchanges of $^4M_{21/2} \leftrightarrow {}^4K_{11/2}$ occurring in the range between levels 95 and 100 and $^4M_{21/2} \leftrightarrow {}^4G_{11/2}$ for 112, 113; and $^4D_{5/2} \leftrightarrow {}^4F_{9/2}$ for levels 132 and 133.

4.3. Energy level fittings employing different conditions

Other calculations were run by varying the fitting conditions, as now described, and the relevant results are listed in table 5.

(a) The $4f^5$ and $4f^5 + 4f^46p$ fittings for a reduced number of energy levels were compared. A fit on a restricted set of 113 levels (up to 29 000 cm^{-1}) yields mean deviations equal to 17.0 and 12.7 cm^{-1} for $4f^5$ and $4f^5 + 4f^46p$ respectively.

(b) Another run was made by missing out the uncertain levels. For the remaining set of 91 levels, the mean deviation is 16.3 and 12.8 cm^{-1} for the $4f^5$ and $4f^5 + 4f^46p$ fittings, respectively.

Table 5. Mean deviations for fittings run with various conditions.

Fitting	Levels	Number	$4f^5$	$4f^5 + 4f^46p$
[1]	All levels	67	16.8	—
1	All levels	135	16.9	14.5
2	Energy limit: 29 000 cm^{-1}	113	17.0	12.7
3	Certified levels	91	16.3	12.8
4	Sextets only	41	12.6	9.9
5	Quartets only	88	18.4	15.2

Table 6. Values of the f-electron CFPs (cm^{-1}) and their variations for fittings run with the various conditions defined in table 5. (Note: B_0^4 and B_0^6 from [1] are transformed into spherical tensors through division by 1.128 and −1.277 respectively. B_0^4 (fp) is equal to 17 600 cm^{-1} in the three calculations. S, sextet; Q, quartet.)

		Reference [1]	This work	
		$4f^5$	$4f^5$	$4f^5 + 4f^46p$
B_0^4 (ff)	Entire set	1793	1855	2293
	Sextets	1689	1814	2262
	Quartets	1794	1880	2333
$(\Delta B_0^4)_S/B_0^4$		−6.3	−2.2	−1.3
$(\Delta B_0^4)_Q/B_0^4$		0.1	1.8	1.8
B_0^6 (ff)	Entire set	277	260	369
	Sextets	236	240	350
	Quartets	275	282	368
$(\Delta B_0^6)_S/B_0^6$		−14.9	−7.7	−5.1
$(\Delta B_0^6)_Q/B_0^6$		−0.7	8.5	0.3

(c) The sextets and the quartets, designating the spin multiplicities, were fitted separately in $4f^5$ and $4f^5 + 4f^46p$ by adjusting the crystal field parameters (CFPs) only. The results gave mean deviations equal to 12.6 and 18.4 cm^{-1} in $4f^5$ for sextets and quartets, respectively; but 9.9 and 15.2 cm^{-1} for these in $4f^5 + 4f^46p$. The fittings which included quartets and doublets gave the same results as with quartets alone.

(d) In an attempt to improve the performance of the method, the distance between the two configurations was tuned. The variation of σ is very flat, and for $\Delta E_{AVE} = 166\,000$ cm^{-1}, σ decreases from 14.5 to 14.3 cm^{-1} for the 135 levels.

(e) Two fittings in $(4f^5 + 4f^46p)$ were run with the certified levels. First, an arbitrary energy limit was set at 29 000 cm^{-1} (table 5, lines 3 and 4), and second, there was no limit. These fittings gave almost the same mean deviations: 12.7 and 12.8 cm^{-1}, which might indicate that the worsening of the performance (with the mean deviation increasing from 12.8 up to 14.5 cm^{-1}) when the whole energy set of 135 levels is considered is due to a few uncertain levels at high energies. This is, however, in contradiction with the fact that the performance in $4f^5$ remains almost the same, whether the entire or a limited dataset is utilized.

The above results are summarized in table 5, whilst table 6 lists the CFP values in the various conditions which have been described.

4.4. Discussion

Several observations can be made from the results of the energy level fits. First, it is shown in table 6, columns 3 and 4, that the strength of the CF depends on the dataset extent. Therefore it

is pointless to debate on physical or chemical grounds the structural reasons for CFP differences unless similar compounds and similar datasets are considered. Second, the last column in table 5 ($4f^5 + 4f^4 6p$: CIACF results) displays in all cases the lowest mean deviations. The specific CI with a single excited configuration $4f^4 6p$ considered here improves in a modest proportion the CF modelling with respect to $4f^5$. Third, in both $4f^5$ and $4f^5 + 4f^4 6p$, the fit on the quartets is 1.5 times poorer than that on the sextets (table 5, lines 6 and 7), with a majority of the latter being situated below 11 000 cm^{-1}. The presence of uncertain and/or inaccurate levels might again be incriminated for the reason. It was suggested in [1] that the different strengths of the CFP as determined from high and low spin states (as shown in table 6 columns 3 and 4) finds its origin in the spin-correlated CF. From the present study, the fractional variations of the CFPs are reported in table 6 for the sextets and the quartets with respect to the global fit, for the two cases of the $4f^5$ and $4f^5 + 4f^4 6p$ fits. The variations of the CFPs are small compared with the case of Tm^{3+} in $Cs_2NaTmCl_6$ [37, 16] where B_0^4(ff) for the singlets is more than 60% larger than for the triplets. The reverse trend (i.e. CFP for triplets > CFP for singlets) was found for Pr^{3+} [15], but for Nd^{3+} CFP for doublets > CFP for quartets [18]. Therefore no consistent trend is apparent along the lanthanide series. The factors responsible for the difference in magnitude of CFPs for states of different spin multiplicity have been discussed by Thorne *et al* [37]. As shown in table 5, different CFPs applied to sextets and quartets do not cancel out the difference in the fitting errors. These errors are due to a predominance of transitions to sextet states occurring in the lower energy range of the spectrum (infrared spectrum mainly) where the fitting of the relevant energy levels is usually much better.

In [1], the manifolds $^6P_{5/2}$ and $^4H_{7/2}$ are quoted as rogue multiplets, with the experimental (versus calculated) splittings being equal to 54 cm^{-1} (versus 27 cm^{-1}) and 209 cm^{-1} (versus 155 cm^{-1}) in $4f^5$. In the $4f^5 + 4f^4 6p$ fitting, the calculated splittings become 36 and 176 cm^{-1}, respectively. This 40% improvement is far better than might be expected from the improvement of the overall mean deviation.

5. Summary and conclusions

The energy level scheme deduced in this study for Sm^{3+} in $Cs_2NaSmCl_6$ shows good agreement with that from the two-photon study of Cs_2NaYCl_6:Sm^{3+} in [1]. The present scheme is more complete and not only includes more levels derived from the infrared absorption spectrum, but extends further into the ultraviolet. The most notable change from the scheme in [1] is for the $^6P_{7/2}$ multiplet term, where the transition to Γ_7 is intense in absorption but quiet in the TPE spectrum.

There have been few previous comprehensive studies of the energy levels of Sm^{3+} in crystals. The most detailed reports are those of $Y_3Al_5O_{12}$:Sm^{3+} [38], $Sr_5(PO_4)_3F$:Sm^{3+} [39], $LiYF_4$:Sm^{3+} [40], SmOCl [41] and [Sm(oxydiacetate)$_3$]·2$NaClO_4$·6H_2O [42], with the correlation CF operators included into the Hamiltonian for several of these in order to improve the fitting. The paucity of reports is due to the complexity of the $4f^5$ configuration. With the parameters in table 4 it is calculated to extend up to 123 782 cm^{-1} ($4f^5$, $^2F_{7/2}$) while the ($4f^4 6p$) configuration begins at 123 652 cm^{-1}. Ryan and Jørgensen [43] assigned the maximum of the charge-transfer band in $SmCl_6^{3-}$ at 232 nm (43 100 cm^{-1}). However, it appears from our results that the configuration which is important in interacting with $4f^5$ is $4f^4 6p^1$, which our fitting calculations place at 31 000 cm^{-1} above the top of the $4f^5$ configuration.

For the $4f^N$ systems Pr^{3+}, Nd^{3+} and Sm^{3+} ($N = 2, 3, 5$) the ratio of the standard deviations in the fittings employing $4f^N + 4f^{N-1}6p$ and $4f^N$ amount to 0.36 [15], 0.41 [18] and 0.86 (present work), respectively. The relative improvement steadily decreases as N increases, probably because the intra-configuration becomes more important than inter-configuration interaction when the number of f-electrons increases. If the pace is conserved, we may expect

the improvement to be negligible for the extended $4f^6$ configuration of trivalent europium in $Cs_2NaEuCl_6$. The fitting error is, however, comparable to the experimental accuracy when taking into account the calibration errors and the noise introduced by uncertain assignments.

Acknowledgments

We acknowledge financial support of this work under the Hong Kong University Grants Commission Research Grant 102304. We are indebted to Dr C S K Mak for technical support in the early part of this work.

References

[1] Thorne J R G, Karunathilake A, Choi H, Denning R G and Luxbacher T 1999 *J. Phys.: Condens. Matter* **11** 7867
[2] Banerjee A K and Schwartz R W 1981 *Chem. Phys.* **58** 255
[3] Schwartz R W and Banerjee A K 1981 *Chem. Phys. Lett.* **79** 19
[4] Foster D R, Richardson F S and Schwartz R W 1985 *J. Chem. Phys.* **82** 618
[5] Tanner P A 1989 *Chem. Phys. Lett.* **155** 59
[6] Thorne J R G, Jones M, McCaw C S, Murdoch K M, Denning R G and Khaidukov N M 1999 *J. Phys.: Condens. Matter* **11** 7851
[7] Berry A J, McCaw C S, Morrison I D and Denning R G 1996 *J. Lumin.* **66/67** 272
[8] Banerjee A K, Stewart-Darling F, Flint C D and Schwartz R W 1981 *J. Phys. Chem.* **85** 146
[9] Luxbacher T, Fritzer H P and Flint C D 1998 *Spectrochim. Acta* A **54** 2027
[10] Luxbacher T, Fritzer H P and Flint C D 1998 *Spectrochim. Acta* A **54** 2099
[11] Luxbacher T, Fritzer H P and Flint C D 1997 *SPIE* **3176** 124
[12] Luxbacher T, Fritzer H P and Flint C D 1998 *J. Alloys Compounds* **275** 250
[13] Morss L R, Siegal M, Strenger L and Edelstein N 1970 *Inorg. Chem.* **9** 1771
[14] Krupski M 1989 *Phys. Status Solidi* a **116** 657
[15] Tanner P A, Mak C S K and Faucher M D 2001 *J. Chem. Phys.* **114** 10860
[16] Faucher M D, Tanner P A and Mak C S K 2004 *J. Phys. Chem.* A **108** 5278
[17] Faucher M D and Tanner P A 2003 *Mol. Phys.* **101** 983
[18] Zhou X, Mak C S K, Tanner P A and Faucher M D 2006 *Phys. Rev.* B **73** 075113
[19] Tanner P A and Siu G G 1992 *Mol. Phys.* **75** 233
[20] Gruen D M and DeKock C W 1966 *J. Chem. Phys.* **45** 455
[21] Karraker D G 1968 *Inorg. Chem.* **7** 473
[22] Henrie D E, Fellows R L and Choppin G R 1976 *Coord. Chem. Rev.* **18** 199
[23] Judd B R 1988 *Handbook of the Physics and Chemistry of Rare Earths* vol 11, ed K A Gschneidner and L R Eyring (Amsterdam: North-Holland) p 137
[24] Huskowska E and Riehl J P 2000 *J. Lumin.* **86** 137
[25] Morrison C E, Leavitt R P and Wortman D E 1980 *J. Chem. Phys.* **73** 2580
[26] Lentz A 1974 *J. Phys. Chem. Solids* **35** 827
[27] Tanner P A, Kumar V V R K, Jayasankar C K and Reid M F 1994 *J. Alloys Compounds* **215** 349
[28] Tanner P A 2004 *Top. Curr. Chem.* **241** 167
[29] Jørgensen C K and Judd B R 1964 *Mol. Phys.* **8** 281
[30] Peacock R D 1975 *Struct. Bonding* **22** 83
[31] Mason S F, Peacock R D and Stewart B 1974 *Chem. Phys. Lett.* **29** 149
[32] Judd B R 1979 *J. Chem. Phys.* **70** 4830
[33] Judd B R 1980 *Phys. Scr.* **21** 543
[34] Faulkner T R and Richardson F S 1978 *Mol. Phys.* **35** 1141
[35] Garcia D and Faucher M 1989 *J. Chem. Phys.* **90** 5280
[36] Cowan R D 1981 *Computer Program RCN31*
[37] Thorne J R, Zeng Q and Denning R G 2001 *J. Phys.: Condens. Matter* **13** 7403
[38] Gruber J B, Zandi B and Reid M F 1999 *Phys. Rev.* B **60** 15643
[39] Gruber J B, Zandi B, Ferry M and Merkle L D 1999 *J. Appl. Phys.* **86** 4377
[40] Wells J-P R, Yamaga M, Han T P J, Gallagher H G and Honda M 1999 *Phys. Rev.* B **60** 3849
[41] Hölsa J and Lamminmäki R-J 1996 *J. Lumin.* **69** 311
[42] Devi A R, Jayasankar C K and Reid M F 1994 *Phys. Rev.* B **49** 12551
[43] Ryan J L and Jørgensen C K 1966 *J. Phys. Chem.* **70** 2845